Journal of Integrative Neuroscience

J. Integr. Neurosci. **2026**; 25(1): 46827
https://doi.org/10.31083/JIN46827

Original Research

Effect of Maternal Hyperglycemia on Cortical Neuronal Migration: Hypofunction of Reelin Signaling

Rocío Valle-Bautista[1], Itzamara Soto-Villanueva[1], Dafne A. Díaz-Piña[1], Vivian A. Chávez Pérez[1], Evelin V. Idiaquez-Hernández[1,2], Daniela Ávila-González[1], Néstor Fabián Díaz[1], Anayansi Molina-Hernández[1,*]

[1]Departamento de Fisiología y Desarrollo Celular, Instituto Nacional de Perinatología Isidro espinosa de los Reyes, Miguel Hidalgo, CP 11000 Ciudad de México, Mexico
[2]Escuela de Medicina y Ciencias de la Salud, Instituto Tecnológico de Monterrey Campus Ciudad de México, CP 14380 Ciudad de México, Mexico
*Correspondence: anayansimolina@gmail.com; anayansimolina@inper.gob.mx (Anayansi Molina-Hernández)
Academic Editors: Woo-Yang Kim and Zhong Chen
Submitted: 23 September 2025 Revised: 5 December 2025 Accepted: 16 December 2025 Published: 23 January 2026

Abstract

Background: Maternal diabetes increases the risk of neurodevelopmental alterations in the offspring, yet the molecular links to early corticogenesis remain unclear. During corticogenesis, radial migration is a coordinated process regulated by Reelin signaling and its disruption has been associated with abnormal cortical patterning. We reanalyze dorsal telencephalon transcriptomes from embryonic day 12 (E12) non-neural tube-defect rat embryos to identify canonical pathways perturbed by maternal hyperglycemia. **Methods**: Gene expression profiles from the dorsal prosencephalon at E12 from control and streptozotocin-treated dams (50 mg/kg at E5.5) were interrogated with Ingenuity Pathway Analysis (IPA). We then assessed Reelin pathway components using quantitative reverse transcription polymerase chain reaction (RT-qPCR), immunohistochemistry, and immunoblotting at E12 and E16, and examined postnatal cytoarchitecture/morphology in the primary motor cortex (M1) at postnatal day zero (P0) and P21 using hematoxylin-eosin and Golgi-Cox staining. All analyses excluded embryos with neural tube defects (NTD) to avoid cofounding by gross malformations. **Results**: IPA revealed Reelin signaling in neurons as the only canonical pathway with a non-zero activation z-score, predicting inhibition in E12 embryos from diabetic rats. Concordantly, protein levels of Reelin (RELN), apolipoprotein E receptor 2/low-density lipoprotein receptor-related protein 8 (ApoER2/LRP8), very low-density lipoprotein receptor (VLDLR), and Disabled Homolog 1 (DAB1) were reduced at E12/E16 (all $p < 0.05$). N-cadherin (N-CAD) showed disrupted radial localization along the ventricular-pial axis despite unchanged total abundance, consistent with impaired neuron-radial glia adhesion/polarity. Postnatally, the M1 showed increased layer I cellularity, ectopic pyramidal neurons, and aberrant laminar organization. **Conclusion**: Maternal hyperglycemia is associated with attenuation of the Reelin signaling pathway and N-CAD mislocalization, providing a mechanistic framework for defective neuronal migration and abnormal lamination that persist into early postnatal life. Focusing on NTD-negative embryos isolates the pathway-specific effects of maternal hyperglycemia and nominates Reelin-pathway hypofunction as a candidate driver of altered fetal cortical patterning.

Keywords: experimental maternal diabetes mellitus; fetal development; mammalian cerebral cortex development; Reelin signaling; fetal programming

1. Introduction

The neocortex acquires its characteristic six-layered architecture during embryogenesis through a highly orchestrated birth of successive cohorts of glutamatergic neurons in the ventricular germinal zones and their radial migration in an inside-out sequence. Early-born neurons settle in the deep layers (V-VI), whereas later-born neurons integrate in the superficial layers (II-IV), enabling precise synaptic connectivity [1].

Before cortical plate (CP) formation, Cajal-Retzius cells (CRs) arise from the cortical hem, septum, and ventral pallidum (pallial-subpallial boundary) and migrate tangentially to the marginal zone (MZ) of the cortical neuroepithelium by approximately embryonic day 10 (E10) in the rat [2–4], where they secrete Reelin (RELN), an extracellular matrix glycoprotein essential for neuroblast radial migration. RELN engages to very low-density lipoprotein receptor (VLDLR) and apolipoprotein E receptor 2 (ApoER2) on migrating neuroblasts and radial glia (RG) cells [5–8], triggering DAB1 (Disabled Homolog 1) phosphorylation through Src-family kinases at least in three tyrosine residues, Y198, Y220, and Y232 [9,10] to regulate cytoskeletal remodeling, adhesion and the migratory "stop" signal near layer I [11], likely through modulating the expression, localization, and activity of N-cadherin (N-CAD). This protein maintains RG polarity and mediates cell-cell adhesion between RG and migrating neuroblasts [7,12].

The VLDLR is expressed in the soma and in the distal region of the neuroblast's leading process (basal process), which will become the apical dendrite of pyramidal neurons [5,8]. This receptor has been implicated in the migration of neuroblasts through the intermediate zone (IZ) to their fi-

nal position near the marginal zone (MZ), thereby preventing the invasion of pyramidal neurons into layer I. VLDLR knockout (KO) mice showed ectopic neurons in the MZ and layer I [5,6].

On the other hand, ApoER2 exhibits its highest expression in the subventricular zone (SVZ), where multipolar neuroblasts accumulate before migration. It has been suggested that its expression decreases as bipolar neuroblasts move through the RG. Hence, it has been postulated that ApoER2 expression might regulate neuroblast morphology before and during migration [8,13].

Interestingly, RELN transgenic mice exhibit macro- and microstructural anomalies in the cerebral cortex, hippocampus, and cerebellum, as well as impaired dendritic development and cognitive deficits [14–16].

Maternal diabetes perturbs embryonic brain development. In a rat streptozotocin (STZ) model, we previously reported in non-neural tube defective embryos and offspring altered intermediate filament integrity of RG cells, disrupted neurogenesis, reduced RELN at the pial surface, and laminar disorganization in the primary motor cortex (M1), alongside polarity defects and decreased excitability in deep-layer pyramidal neurons [17,18]. In humans, gestational diabetes is associated with motor and language development, increased risk for neurodevelopmental disorders [19–21], as well as autism and schizophrenia [22–25].

Here, we hypothesized that maternal hyperglycemia impairs radial migration by attenuating RELN/DAB1 signaling and disrupting neuron-glia interactions. To specifically isolate pathway disruption from gross developmental delay, we focused our analysis exclusively on embryos without neural tube defects. We therefore: (1) reanalyzed the rat dorsal prosencephalon transcriptome at embryonic day 12 (E12; https://www.ebi.ac.uk/fg/annotare/, accession number E-MTAB-15111) using Ingenuity Pathway Analysis (IPA) to prioritize canonical pathways; (2) quantified RELN, ApoER2, VLDLR, and phospho- DAB1 (p-DAB1) at E12 and E16; (3) assessed N-CAD distribution and abundance, and (4) examined postnatal M1 cytoarchitecture and upper-layer neuron markers.

2. Methods and Living Beings

All experiments were carried out following the "Guide for the Care and Use of Laboratory Animals" (NIH 80-23, revised 1978), the Official Mexican Standard for the Production, Care, and Use of Laboratory Animals (NOM-062-ZOO-1999), ARRIVE guidelines, and were approved by the Institutional Committee for the Care and Use of Laboratory Animals (CICUAL) and the Research, Ethics, and Biosafety Committees of the Instituto Nacional de Perinatología (protocol 2018-1-146).

Adult Wistar rats (230–300 g) were obtained from the Animal Facility of the Instituto Nacional de Perinatología Isidro Espinosa de los Reyes (INPer), Mexico. Animals were housed (22 ± 2 °C) on a 12:12 h light/dark cycle, relative humidity of 40%, and *ad libitum* water and food. The females were placed with a sexually mature male during the dark phase, and pregnancy was confirmed by the presence of spermatozoa in a vaginal smear (E0.5).

At E5.5, dams assigned to the diabetic group (Db) received a single intraperitoneal dose of streptozotocin (STZ; 50 mg/kg; S0130-5G, Sigma-Aldrich, St. Louis, MO, USA) dissolved in 100 mM citrate buffer (pH 6.4) prepared using citric acid (Cat. 40513, HYCEL, Zapopan, Jalisco, Mexico) and sodium citrate (Cat. 5584UB, Sigma-Aldrich). The pH was adjusted to 6.4 with NaOH. The control group (Ctrl) received the vehicle. Glycemia was determined in both groups 48 h after induction and before euthanasia, using a drop of blood obtained by puncture of the caudal vein and an electronic glucometer (Accu-Chek Performa, Roche, Basel, Switzerland). Rats with glycemia $\geq$200 mg/dL were defined as Db; vehicle-treated dams with 90–120 mg/dL were included in the Ctrl group. Embryos with NTD (pre-specified criteria) were excluded.

For embryonic tissue collection (E12 and E16), pregnant rats were deeply anesthetized with sevoflurane at 4.5% (S2912J17, Savannlab®, Piramal Critical Care, Inc., Bethlehem, PA, USA) until loss of reflexes and then euthanized by decapitation. The embryos were immediately removed and rapidly processed to prevent contamination, and then fixed or dissected for the collection of prosencephalon/dorsal telencephalon tissue at 4 °C using sterile solutions. For postnatal stages (P0 and P21), pups were euthanized by decapitation using a rodent guillotine. Decapitation was selected to prevent chemical contamination of brain tissue, which is critical for downstream molecular and histological analyses of neurodevelopment. All procedures, including euthanasia, were performed by trained personnel using sharp, calibrated instruments.

2.1 Tissue Collection and Processing

Pregnant dams were deeply anesthetized with sevoflurane (4.5%, S2912J17, Savannlab®, Piramal Critical Care, Inc.) until complete loss of reflexes, confirmed by the absence of corneal reflexes and response to tail pinch, and were subsequently euthanized by decapitation using a sharp, calibrated guillotine at E12 and E16. All procedures were performed by trained personnel. Embryos were recovered by cesarean section, washed with sterile PBS (4 °C), and fixed by immersion in sterile Bouin's solution (15:15:1 saturated picric acid solution (SPC-P1145-500G, Spectrum Chemicals, New Brunswick, NJ, USA): 40% formalin (P6148, Sigma-Aldrich): glacial acetic acid (1005706, Sigma-Aldrich). For paraffin histology and immunofluorescence at embryonic stages, tissue was dehydrated by sequentially placed in alcohol gradients of 70%, 80%, 90%, 96%, and 100% for 1 h each, passed to xylol-alcohol 1 h, xylol for 5 min, and embedded in paraffin (Paraplast®, Leica Biosystem, Richmond, IL, USA) for 4 h. Coronal sections (10 µm) containing the prosen-

Table 1. Primary antibodies.

Antibody	Functional description	Dilution (IF)	Dilution (WB)	Host	Supplier and catalog no.
Reelin	Stop signal for migrating neuroblast	1:100	-	Mouse	Millipore MAB5364
VLDLR	Reelin receptor	1:200	1:30	Mouse	Santa Cruz 18824
ApoER2	Reelin receptor	1:500	1:250	Rabbit	Abcam Ab108208
P-DAB1 (Tyr 232)	Reelin effector protein	1:30	1:125	Rabbit	My BioSource MBS9600801
N-Cadherin	Adhesion Molecule	1:200	1:250	Rabbit	GeneTex GTX127345
β-Actin	cytoskeletal protein used as an internal control	-	1:1000	Rabbit	GeneTex GTX109639
β-Actin	cytoskeletal protein used as an internal control	-	1:1000	Mouse	GeneTex GTX82559

IF, immunohistofluorescence; WB, western blot; VLDLR, very low-density lipoprotein receptor; ApoER2, apolipoprotein E receptor 2; DAB1, disabled homolog 1.

cephalon/telencephalon were obtained using a microtome (MICROM320, Heidelberg Instruments, Heidelberg, Germany) and recovered in glass slides coated with Poly-L-lysine (P8920, Sigma-Aldrich).

Neonates (postnatal day zero; P0) and P21 offspring were euthanized by decapitation; brains were fixed by immersion in Bouin's solution, cryoprotected in 30% sucrose, embedded in TissueTek, frozen, and 10 µm coronal sections were obtained using a cryostat (Leica CM1850 UV, Wetzlar, Germany) to sample the primary motor cortex (M1).

2.2 Immunohistofluorescence

Sections were washed three times for 10 min in PBS, permeabilized, and blocked (PBS, 10% normal goat or horse serum, and 0.3% Triton X-100; 1 h), and then treated with TrueBlack (23007, Biotium, Hayward, CA, USA) to quench autofluorescence. Primary antibodies (Table 1) were incubated overnight at 4 °C in PBS containing 10% serum, followed by washes and incubation with species-appropriate secondary antibodies (Table 2) for 1 hour at room temperature. Nuclei were counterstained with 4′,6-diamidino-2-phenylindole (DAPI; 1 µg/mL, 8 min, D9542, Sigma-Aldrich), washed, and mounted in Aqua Poly/mount (Polyscience, 18606-100, Warrington, PA, USA).

Quantitative immunofluorescence for VLDLR and ApoER2 was performed using an infrared scanner system (Odyssey CLx; LICORbio, Lincoln, NE, USA) and the Image Studio version 4.0 software (LICORbio). Six consecutive coronal sections per litter (experimental unit; n) were analyzed, for a total of n = 4 per group. The fluorescent signal obtained for each receptor was normalized using DRAQ5 (1, 5-bis{[2-(di-methylamino)ethyl]amino}-4, 8-dihydroxyanthracene-9, 10-dione. 5 µM; 1:1000, ab108410, Abcam, Cambridge, UK), and the results were expressed as a percentage of the Ctrl group. Representative images were processed using Adobe Photoshop CS6 (Adobe Inc., San Jose, CA, USA).

2.3 Western Blot

The dorsal telencephalon at E16 was micro-dissected and pooled from four embryos per litter to yield a sample size of n = 1, for a total n = 3 per group. Tissue was homogenized using a Polytron PT 2100 homogenizer (Kinematica, Malters, Switzerland) in a lysis buffer (HEPES 20 mM, $MgCl_2$ 1.5 mM, KCl 10 mM, DTT 1 mM) containing a protease and phosphatase inhibitor cocktail (A32961, Thermo Scientific, Waltham, MA, USA). After centrifugation (13,000 $\times$g at 4 °C for 10 min), supernatants were recovered and protein quantified using the Bradford assay [26]. Samples (40–80 µg) were separated in 10% polyacrylamide gels by electrophoresis using the Mini-Protean II system (Bio-Rad, Hercules, CA, USA).

Proteins were transferred to nitrocellulose membranes (AmershamTM Hybond TM-ECL, Buckinghamshire, UK), using the Trans-Blot R semi-dry transfer cell system (Bio-Rad) as previously described (Villanueva, 2008), unspecific antibodies binding was blocked with a commercial TBS blocking buffer (927-60001, LICORbio), incubated overnight at 4 °C with the primary antibodies (Table 1), membranes were washed and incubated with the following LICORbio infrared antibodies (Table 2). The corresponding bands were quantified using ImageStudio software version 4.0 (LICORbio). Signals were normalized to β-actin and expressed as a percentage of Ctrl. Original WB dates are in the **Supplementary Material-Original WB**.

2.4 Histology: Hematoxylin-Eosin and Golgi-Cox

To assess potential invasion of layer I (molecular layer) by neurons, coronal sections from male offspring (P0 and P21; n = 3) brains were stained with hematoxylin-

Table 2. Secondary antibodies.

Antibody	Dilution (IF)	Dilution (WB)	Host	Species Reactivity	Supplier and catalog no.
AlexaFluor 488	1:1000	-	Goat	Rabbit	ThermoFisher A11034
AlexaFluor 568	1:1000	-	Goat	Mouse	ThermoFisher A11031
AlexaFluor 568	1:1000	-	Goat	Rabbit	ThermoFisher A11036
IRDye 800CW	-	1:10,000	Goat	Rabbit	LICORbio IRDye 926-32211
IRDye 800RD	-	1:10,000	Goat	Mouse	LICORbio 926-32210
IRDye 680RD	-	1:10,000	Goat	Mouse	LICORbio 926-68070
IRDye 680RD	-	1:10,000	Goat	Rabbit	LICORbio 926-68071
IRDye 800CW	1:200	-	Donkey	Rabbit	LICORbio 926-32213
IRDye 800CW	1:200	-	Donkey	Mouse	LICORbio 926-32212
IRDye 680RD	1:200	-	Donkey	Mouse	LICORbio 926-68072
IRDye 680RD	1:200	-	Donkey	Rabbit	LICORbio 926-68073

eosin following standard protocols. Neuronal identity and morphology were evaluated using FD Rapid GolgiStain™ (PK401, FD Neurotechnologies, Columbia, MD, USA) on coronal sections (P0: 60 µm; P21: 20 µm) following the manufacturer's instructions.

Micrographs from both preparations were obtained at a 10× magnification. For hematoxylin-eosin, reconstructions of two (P0) or six (P21) images were assembled in Photoshop. For Golgi-Cox-stained preparations, P21 coronal sections were used to obtain ≥20 micrographs at different focal planes per slide to follow neuron arborization. The images were further processed in Photoshop, scaled, and printed. Complete neurons were then scanned and analyzed.

Because the Golgi-Cox impregnation labels only a random subset of neurons, we used these sections strictly to identify the neuronal phenotype (pyramidal morphology) and to estimate relative increase in ectopic pyramidal neurons in layer I, while absolute cellularity was quantified separately from H&E sections. The method provides high-resolution visualization of the soma, dendritic arbors, and spines in a sparsely labeled population, yielding semi-quantitative information on neuronal morphology and distribution. To minimize selection bias, sampling was uniform across groups, using matched rostro-caudal levels and cortical regions, identical ROI (region of interest) dimensions, and fixed acquisition parameters.

Analyses were performed blinded to the group, with predefined inclusion/exclusion criteria (complete impregnation and intact soma), and results are reported as per-ROI estimates.

2.5 Transcriptomic Re-Analysis

Differential expression results from the dorsal prosencephalon (E12, Ctrl vs Db) previously analyzed with ShinyGO v0.741 (https://bioinformatics.sdstate.edu/go74/) [21] were reanalyzed in IPA (Qiagen; Redwood City, CA, USA) to identify canonical pathways, upstream regulators, and disease/function annotations. Significance was assessed by Fisher's exact test ($-\log p > 1.3$) and activation state by IPA z-score.

2.6 Statistical Analysis

Data are presented as mean ± standard error of the mean (SEM). Unpaired Student's *t*-test was used for planned comparison between Ctrl and Db at matched ages. The litter served as a biological unit for section-based and Western blot analyses. A threshold of $p < 0.05$ was considered significant. Exact n values are reported per experiment. Multiple endpoints within the priori RELN pathway were tested; we interpret the results in the context of a strong prior hypothesis; nevertheless, readers are cautioned that nominal *p*-values are presented. Statistical analysis and graphics were performed using GraphPad Prism version 9 (GraphPad Software, Inc., San Diego, CA, USA).

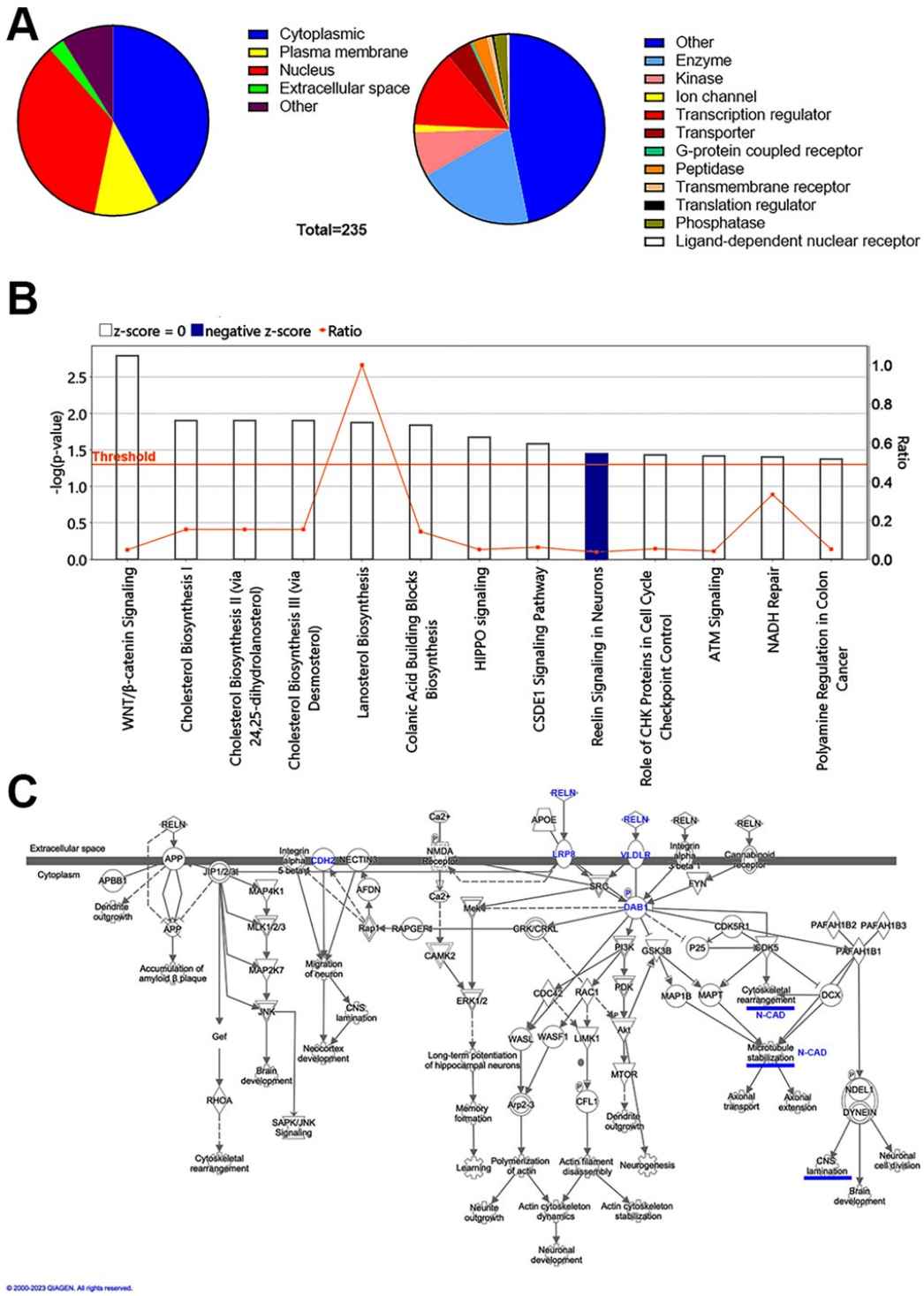

Fig. 1. Canonical pathway enrichment highlights predicted inhibition of Reelin signaling at E12 in embryos from diabetic dams. (A) Pie charts showing subcellular localization (left) and protein classes (right) for the 235 differentially expressed genes in dorsal prosencephalon at E12 (diabetic vs control). (B) Ingenuity Pathway Analysis (IPA) of canonical pathways. Bars show –log *p* (left y-axis); the horizontal orange line marks the significance threshold (–log *p* = 1.3; i.e., *p* = 0.05). Bar color indicates predicted activation state from IPA z-scores: orange, positive z (predicted activation); blue, negative z (predicted inhibition); white, z = 0 (no prediction). The right y-axis shows the ratio of differentially expressed genes in our dataset to all genes in each pathway. (C) Schematic of the IPA Reelin signaling pathway derived from the transcriptomic analysis. Nodes are color-coded by fold-change (red, up; green, down). Key regulators of migration and polarity that were experimentally validated are highlighted in blue: Reelin (RELN), phosphorylated (PDAB1), ApoER2/LRP8, VLDLR, and N-Cadherin/Cadherin-2 (N-CAD/CDH2). Solid lines depict curated direct interactions; dashed lines represent indirect or predicted associations in the IPA knowledge base.

Table 3. Canonical pathways enriched in the dorsal prosencephalon in embryonic day 12 from diabetic dams (IPA).

Ingenuity Canonical Pathways	–log *p*	Ratio
Wnt/β-catenin Signaling	2.79	0.0488
Cholesterol Biosynthesis I	1.90	0.1540
Cholesterol Biosynthesis II (via 24,25-dihydrolanosterol)	1.90	0.1540
Cholesterol Biosynthesis III (via Desmosterol)	1.90	0.1540
Lanosterol Biosynthesis	1.87	1.0000
Colanic Acid Building Blocks Biosynthesis	1.84	0.1430
Hippo signaling	1.67	0.0506
CSDE1 Signaling Pathway	1.58	0.0625
Reelin Signaling in Neurons	1.45	0.0368
Role of CHK Proteins in Cell Cycle Checkpoint Control	1.43	0.0545
ATM Signaling	1.42	0.0421
NADH Repair	1.40	0.3330
Polyamine Regulation in Colon Cancer	1.37	0.0517

CSDE1, cold shock domain containing E1; CHK, checkpoint kinase 1; ATM, ataxia-telangiectasia mutated; NADH, nicotinamide adenine dinucleotide (reduced form).

3. Results

The IPA analysis of E12 dorsal prosencephalon transcriptome from Ctrl and Db pregnant rats [27] revealed 235 genes differentially expressed (129 downregulated and 106 upregulated; **Supplementary Table 1**). Proteins encoded by these genes are predominantly localized to the cytoplasm, nucleus, and plasma membrane (Fig. 1A), and are enriched for enzymes and transcription regulators, among others (Fig. 1B and **Supplementary Table 1**). Of the 13 Ingenuity canonical pathways detected, Reelin Signaling in Neurons was the only pathway with a non-zero z score and a significant but modest enrichment (–log *p* value = 1.45), with a negative z score predicting inhibition in the Db group (Fig. 1B, Table 3). This pathway falls within the categories of "Neurotransmitters and Other Nervous System Signaling; Organismal Growth and Development" IPA disease/functions annotations highlighted "Cell Morphology; Cellular Assembly and Organization; and Cellular Development" (**Supplementary Table 2**), supporting a model of impaired neuronal migration during corticogenesis in embryos from Db rats.

The Reelin signaling in Neurons pathway diagram in IPA (Fig. 1C) centers on RELN binding to its canonical receptors ApoER2 (LRP8; low-density lipoprotein receptor-related protein 8) and very low-density lipoprotein receptor (VLDRL), which engage intracellular cascades controlling neuronal migration, cortical lamination, cytoskeleton dynamics, differentiation, and dendritic growth. IPA also depicts functional interaction with additional membrane proteins/pathways (e.g., APP; amyloid precursor protein, integrins, selected GPCRs; G protein-coupled receptors), which modulate but are not primary RELN receptors. Although few pathway nodes were transcriptionally altered in our dataset (e.g., downregulation of CAMK2; calcium/calmodulin-dependent protein kinase type II, and AKT; protein Kinase B), these results prioritized post-transcriptional or post-translational defects in RELN signaling for experimental validation. We therefore evaluated RELN, ApoER2, VLDLR, activated Dab1 (p-DAB1), and the distribution of N-CAD in the cortical neuroepithelium at E12 (the onset of pyramidal neurogenesis/migration) and E16 (mid-corticogenesis) [28].

At E12, immunofluorescence showed RELN mark and p-DAB1 in Ctrl cortical neuroepithelium, consistent with active RELN signaling (Fig. 2A–D). In embryos from the Db group, both marks were reduced, indicating a substantial decrease in the activation of this pathway (Fig. 2B). Quantification demonstrated decreases from 100 $\pm$ 36.6% to 18.5 $\pm$ 7.4% for RELN and from 100 $\pm$ 36.0% to 19.3 $\pm$ 13.4% for p-DAB (Fig. 2C,D).

To determine if this deficit persisted, we examined E16 telencephalon (Fig. 3A–D). In the Ctrl, RELN labeling extended from the basal to apical regions without reaching the VZ. In the Db group, RELN labeling was scarce along the cortical neuroepithelium, reduced to 26.2 $\pm$ 0.3% of the Ctrl (i.e., 73.8% reduction; Ctrl: 100 $\pm$ 27.2%; Fig. 3B,C). Western blot confirmed decreased RELN (53.6 $\pm$ 5.3% of the Ctrl; Fig. 3D) and p-DAB1 (51.5 $\pm$ 2.3% of the Ctrl; Fig. 3E), indicating sustained attenuation of RELN/DAB1 signaling until E16.

Because RELN regulates neuron-RG adhesion and polarity [29,30], we evaluated N-CAD at E16 (Fig. 4). In the Ctrl, N-CAD exhibited a radial pattern, enriched at apical (VZ) and basal (MZ) neuroepithelium, consistent with expression in RG and migrating neuroblasts (Fig. 4A). In the Db group, N-CAD radial pattern was disrupted with a pronounced reduction of its immunofluorescence signal within the cortical neuroepithelium (8.2 $\pm$ 24.4% vs 100 $\pm$ 16.9% of the Ctrl; Fig. 4B). In contrast, Western blot showed no significant difference in total N-CAD protein

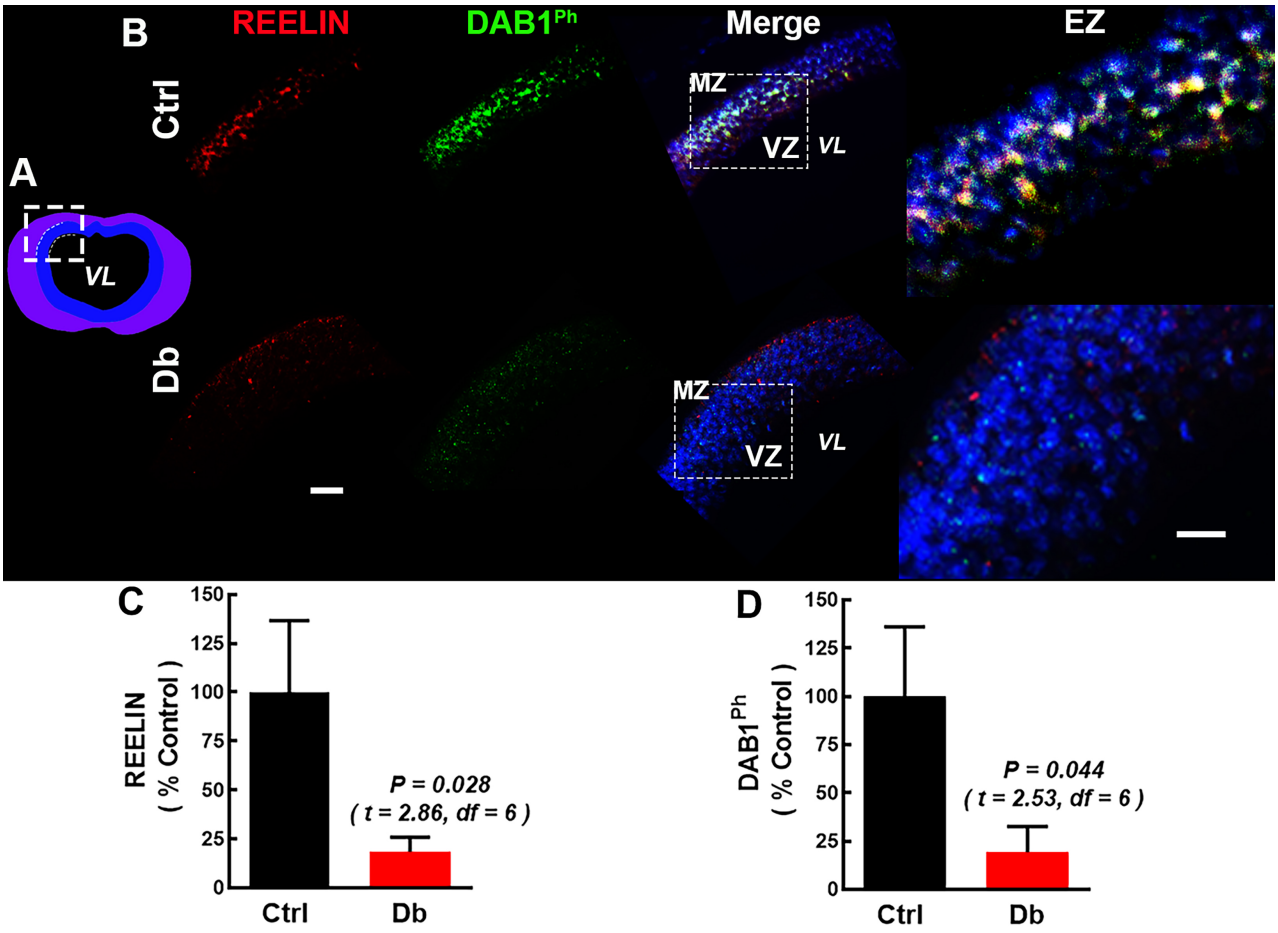

Fig. 2. Reelin and p-DAB1 are reduced in the dorsal prosencephalon at E12 in embryos from diabetic dams. (A) Schematic coronal view of the rat forebrain at E12; the white dashed box marks the dorsal region analyzed. (B) Representative 20× images from control (Ctrl) and diabetic (Db) rat embryos showing Reelin (red), p-DAB1 (pY232) (green), and DAPI (blue). Right panels: electronic zoom (EZ, 300%) of the boxed areas. MZ, marginal zone; VZ, ventricular zone; VL, ventricular lumen. Scale bars: 100 µm (20×), 25 µm (EZ). (C,D) Quantification of Reelin and p-DAB1 immunofluorescence in Ctrl (black bars) and Db (red bars) groups. Values are expressed as percentage of Ctrl (means ± SEM; n = 4 litters/group; six consecutive sections/litter). Two-tailed unpaired Student's *t*-test; *p* values shown on graphs. All images for a given marker were acquired and processed with identical settings. p-DAB1, phospho-disabled homolog 1; DAPI, 4′,6-diamidino-2-phenylindole.

between groups (Fig. 4C), indicating mislocalization rather than loss of abundance.

We next quantify RELN receptors at E16 by immunofluorescence and Western blot (Fig. 5A–F and Fig. 6A–F). ApoER2 was decreased in the Db group relative to the Ctrl by both immunofluorescence (17.1 ± 0.2% from 100 ± 19.1% of the Ctrl) and scanner quantification (10.3 ± 5.6% from 100 ± 20.0% of the Ctrl; Fig. 5B–E). VLDLR showed near-abolition of immunofluorescence (0.2 ± 0.001% from 100 ± 30.7% of the Ctrl), while the infrared scanner indicated a reduction to 26.1 ± 7.8% from 100 ± 20.2% of the Ctrl (Fig. 6B–E). Despite methodological differences in dynamic range and normalization, all assays consistently supported directionally reduced receptor levels in the Db group.

To assess postnatal consequences, we examined M1 cytoarchitecture at P0 and P21 using hematoxylin-eosin, Golgi-Cox, and upper-layer markers (Figs. 7,8). Hematoxylin-eosin revealed increased cellularity in layer I (molecular layer) of Db offspring at P0 and P21 (1.8 ± 0.08-fold and 1.2 ± 0.05-fold vs Ctrl, respectively; matched ROIs; Fig. 7A–D). Golgi-Cox at P21 confirmed ectopic pyramidal neurons in layer I with 3.9-fold more neurons than the Ctrl group (Fig. 7B',B",D). These findings indicate defective termination of radial migration at the MZ and suggest insufficient elimination of aberrantly positioned neurons.

Finally, we mapped upper-layer neurons by Cut Like Homeobox 1 (CUX1) and Special AT-Rich Sequence-Binding Protein 2 (SATB2) immunofluorescence at P0 and P21 (Fig. 8A–I). As expected, Ctrl neonates (P0) exhibited deeper CUX1+ neurons (indicating ongoing migration), with predominantly II-IV expression at P21 (Fig. 8B,H). In Db, CUX1+ neurons at P0 were abnormally superficial; at

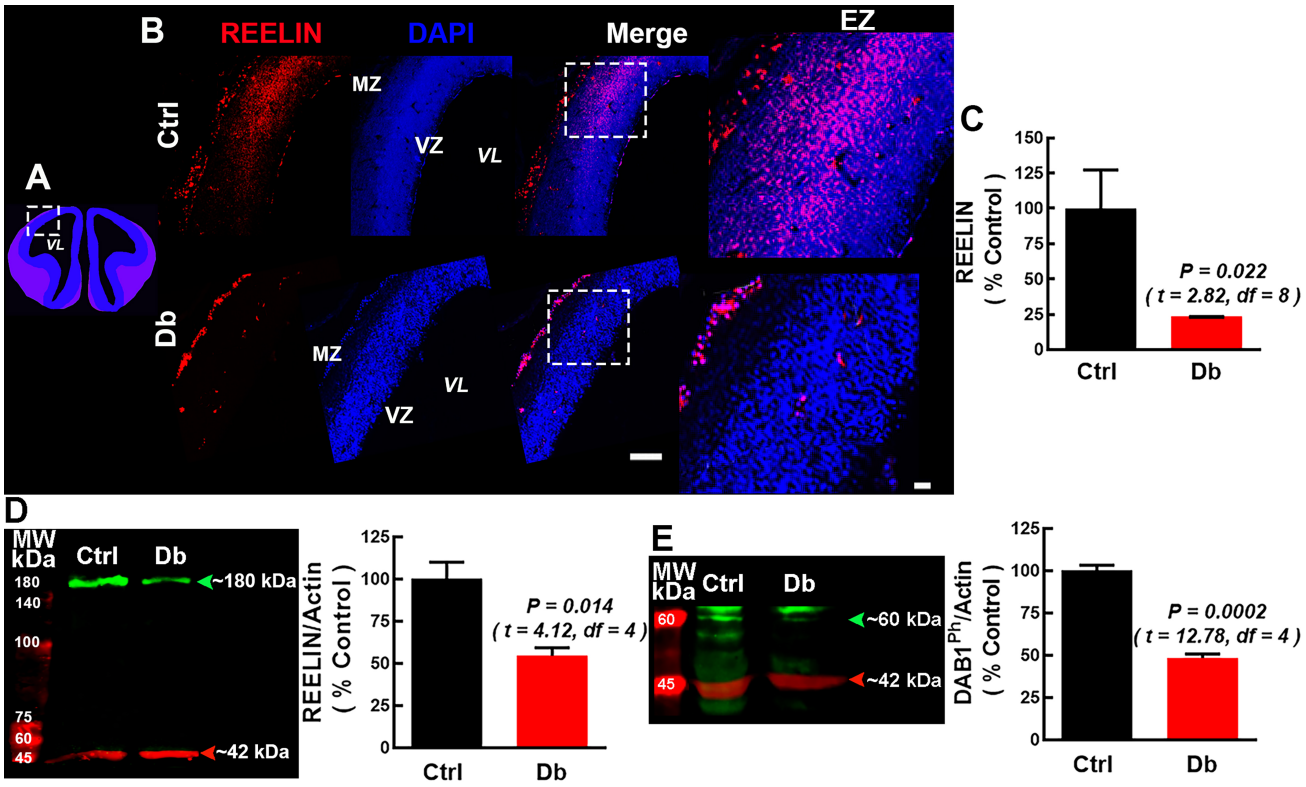

Fig. 3. Reelin/p-DAB1 is attenuated at E16 in embryos from diabetic dams. (A) Schematic coronal view of the rat telencephalon at E16; dashed box indicates the analyzed region. (B) Representative 10× reconstructions (three fields) showing Reelin (red), DAPI (blue), and merge channels in the dorsal telencephalon of embryos from control (Ctrl) and diabetic (Db) rats. Right panels are electronic zoom of boxed regions: (EZ, 300%). Scale bars = 100 µm (10×) and 25 µm (EZ). MZ, marginal zone; VZ, ventricular zone; and VL, ventricular lumen. (C) Semi-quantitative Reelin immunofluorescence in Ctrl (black bar) and Db (red bar) groups expressed as percentage of Ctrl. Values are the mean ± SEM (n = 5 litters/group). (D,E) Immunoblots at E16 for Reelin (D, ~180 kDa, green), and p-DAB1 (~60 kDa, green) with β-actin (~42 kDa, red) as loading control, beside each blot is the quantification of the corresponding bands expressed as percentage of Ctrl (mean ± SEM; n = 3 litters/group; one pooled tissue sample per litter). M.W. molecular-weight ladder. Two-tailed unpaired Student's *t*-test was performed for all comparisons; *p* values are shown.

P21, CUX1 signaling encroached upon layer I, and overall CUX1 intensity was higher than Ctrl (Fig. 8D,E). For SATB2, Ctrl showed labeling above layer V at P0 with minimal layer I signal by P21 (Fig. 8C,I). In Db, SATB2+ neurons were more broadly distributed across cortical depth at P0; by P21, SATB2 labeling no longer extended into layer I, yet overall SATB2 intensity remained elevated relative to Ctrl (Fig. 8F,G). Together with hematoxylin-eosin and Golgi-Cox, these data indicate scrambled-like lamination and ectopic layer I neurons consistent with attenuated RELN signaling.

4. Discussion

In this study, we combined pathway-level transcriptomics with anatomical and biochemical readouts to interrogate how maternal hyperglycemia perturbs early corticogenesis. IPA of E12 dorsal cortex revealed Reelin Signaling in Neurons as the sole canonical pathway with a non-zero activation z-score, predicting inhibition in embryos from diabetic dams. The implicated functional categories—cell morphology, cellular assembly/organization, and cellular development—are concordant with our previous ShinyGO analysis and with experimental evidence for mitotic spindle and cytoskeletal alterations under hyperglycemic conditions *in vivo* and *in vitro* [27].

We validated this prediction at the protein level: RELN, its receptors VLDLR and ApoER2/LRP8, and p-DAB1 were all reduced at E12 and E16 in embryos from Db dams. The attenuation of these components was maintained from E12 to E16, suggesting that this is not due to a simple developmental delay but a chronic deficit in Reelin signaling. These convergent changes support a model in which attenuated RELN → ApoER2/VLDL → DAB1 signaling compromises radial migration. Mechanistically, RELN released by Cajal-Retzius cells engages ApoER2/VLDLR on migrating neurons and RGC, promoting receptor clustering and DAB1 phosphorylation by Src family kinases [14,24]. Downstream, this cascade regulates cytoskeletal remodeling, neuronal polarity, and adhesion in part through N-CAD and small GTPases [29].

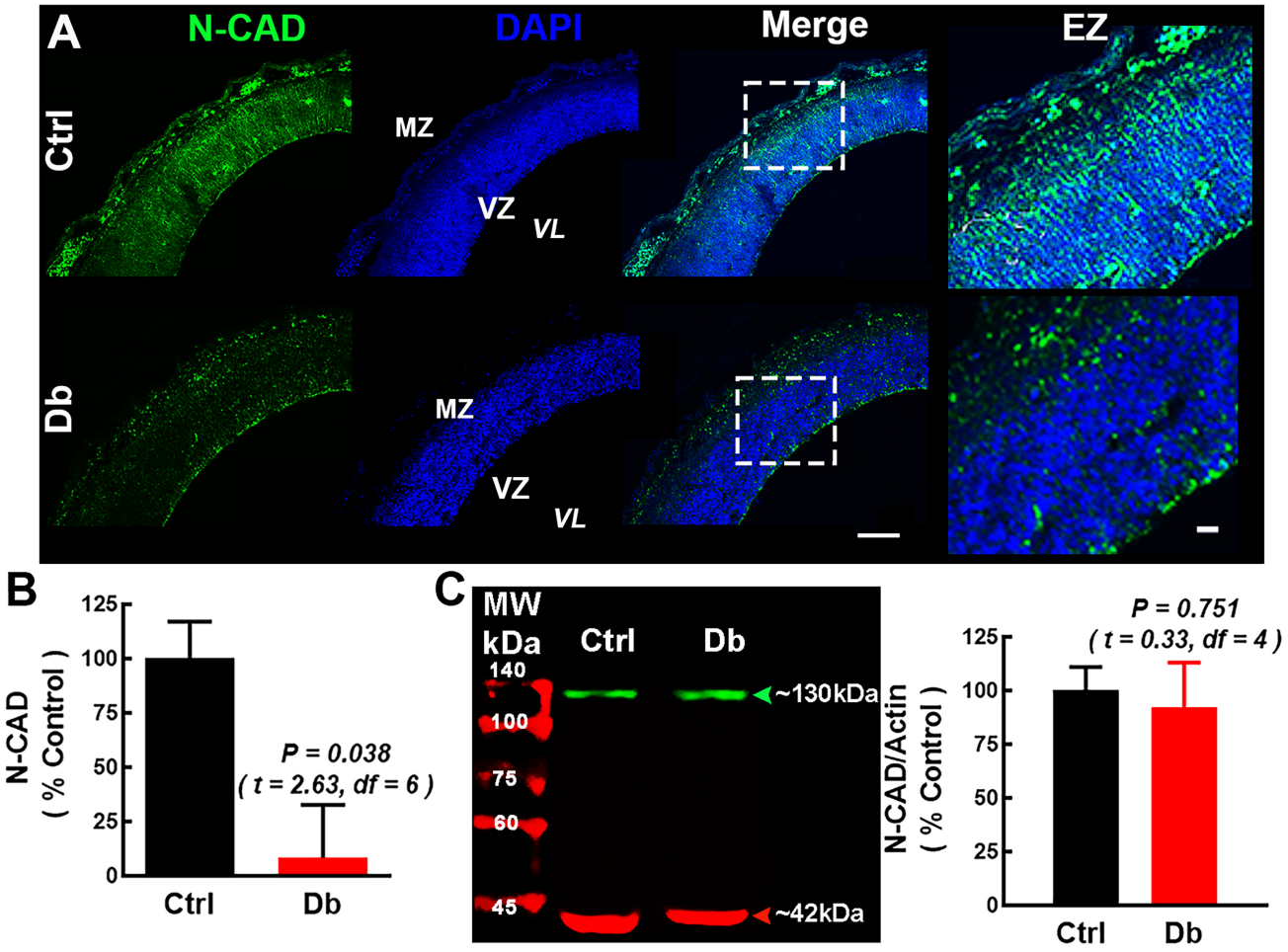

Fig. 4. N-Cadherin mislocalization at E16 in embryos from diabetic dams. (A) Representative 10× reconstructions (three fields) of N-Cadherin (N-CAD; green) with DAPI (blue) in control (Ctrl) and diabetic (Db); right panels show EZ (300%) from the same anatomical area as in Fig. 3A. Scale bars = 100 µm (10×) and 25 µm (EZ). MZ, marginal zone; VZ, ventricular zone; and VL, ventricular lumen. (B) Semi-quantitative N-Cadherin (N-CAD) immunofluorescence in Ctrl (black bar) and Db (red bar) groups expressed as percentage of Ctrl. Values are the mean ± SEM (n = 3–5 litters/group). (C) Immunoblot for N-CAD (~130 kDa) with β-actin (~42 kDa, as loading control), beside the blot in the quantification of the corresponding band expressed as percentage of Ctrl (mean ± SEM; n = 3 litters/group). Two-tailed unpaired Student's *t*-test; *p* values are shown.

Importantly, neither *RELN*, *VLDLR*, *ApoER2* and *N-CAD* mRNA showed significant downregulation in our differential expression dataset [28], despite robust protein-level decreases. This dissociation strongly suggests post-transcriptional regulation. A plausible mechanism involves microRNAs (miRNAs) targeting 3′ untranslated region (3′UTR); e.g., miR-200c has been reported to repress RELN in ischemic paradigms [31] and TargetScan (v7.2) predicts conserved miR-200c-3p/miR-200b-3p sites in the RELN 3′UTR. Consistent with this, we previously identified miR-200b-3p in maternal serum during gestational diabetes [32]. Future studies should directly test this axis using RELN-3′UTR luciferase reporters, miRNA mimic/inhibitor manipulations, and qPCR/immunoblot validation of RELN and receptor expression.

At the tissue level, N-CAD exhibited marked mislocalization along the cortical wall in diabetic embryos and loss of the normal radial pattern at the VZ/MZ. The mislocalization occurred despite total N-CAD protein abundance remaining unchanged by Western blot, indicating a defect in localization, rather than a change in protein expression. Given N-CAD's essential role in neuron-RGC adhesion and radial translocation, its mislocalization likely exacerbates migratory failure and contributes to aberrant lamination. These observations dovetail with our and others' prior findings of cytoskeletal defects, altered neurogenesis, and impaired dendritic maturation/excitability in offspring of diabetic dams [17,18,27,33].

Postnatally, we observed ectopic pyramidal neurons in layer I and disorganization of upper-layer markers in M1. Reduced VLDLR provides a parsimonious explana-

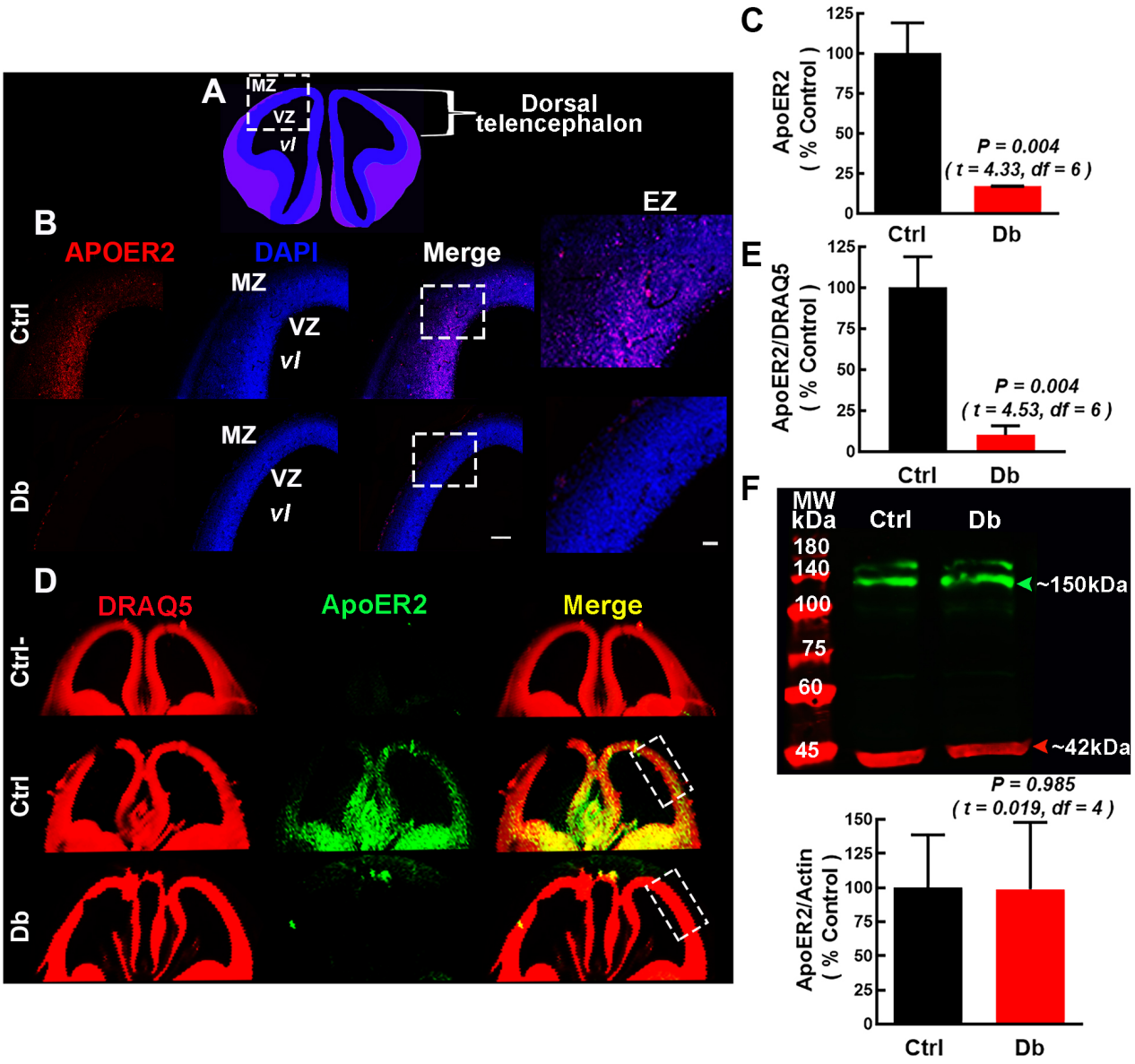

Fig. 5. ApoER2/LRP8 is decreased at E16 in embryos from diabetic dams. (A) Schematic coronal view of E16 telencephalon; dashed box marks the region of intrest. (B) Representative 10× images ApoER2 (red), DAPI (blue), merge channels, and electronic zoom (EZ; 300%) from boxed areas in control (Ctrl; top) and diabetic (Db; bottom). MZ, marginal zone; VZ, ventricular zone. Scale bars: 100 (10×), 25 µm (EZ). (C) Semi-quantitative ApoER2 immunofluorescence (% of Ctrl; mean ± SEM, n = 3–5 litters/group). (D) Infrared scanner images showing ApoER2 (green), DRAQ5 (1, 5-bis{[2-(di-methylamino)ethyl]amino}-4, 8-dihydroxyanthracene-9, 10-dione) nuclei (red; internal normalizer), and merged from frontal coronal; Ctrl- = no primary antibody control. (E) Quantification of ApoER2/DRAQ5 fluorescence ratios in the boxed ROI (% of Ctrl; mean ± SEM; n = 3–5 litters/group). (F) Immunoblot for ApoER2 (~150 kDa) with β-actin control (~42 kDa, top) and quantification (bottom) as % of Ctrl (mean ± SEM; n = 3 litters/group). Two-tailed unpaired Student's *t*-test; *p* values shown.

tion for faulty "stop" signaling at the marginal zone, consistent with layer I over-migration in VLDLR-null models [5]. Decreased ApoER2 may impair the multipolar-to-bipolar transition in the IZ/SVZ, aligning with aberrant CUX1 positioning and broadening SATB2 distributions [6,10,13]. Notably, by P21, SATB2 labeling no longer extended into layer I, even though Golgi-Cox revealed ectopic layer I pyramidal neurons; this suggests a subset of ectopic neurons are Reelin-negative (deep-layer identity) or that marker expression is misregulated. This is supported by the fact that no periventricular heterotopia was observed (**Supplementary Fig. 1**).

Together, these results support a scrambled-like lamination phenotype driven, at least in part, by weakened RELN signaling. However, the causal nature of this relationship warrants further investigation into its mecha-

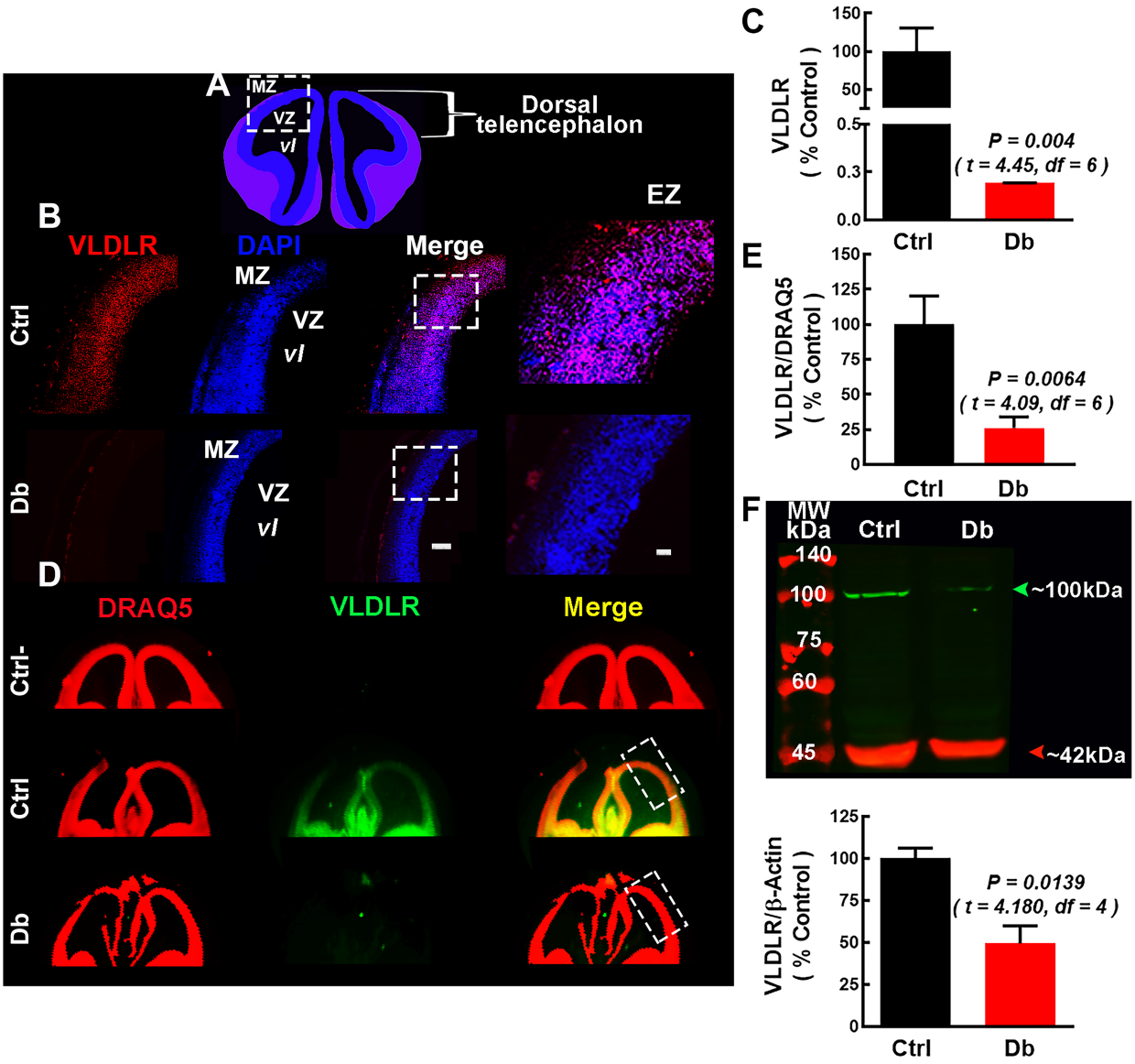

Fig. 6. VLDLR is decreased at E16 in embryos from diabetic dams. (A) Schematic coronal view of E16 telencephalon; dashed rectangle marks the dorsal ROI. (B) Representative images (10×) showing VLDLR (red), DAPI (blue), merges, and electronic zoom (EZ; 300%) from the boxed region in control (Ctrl) and diabetic (Db). MZ, marginal zone; VZ, ventricular zone. Scale bars: 100 µm (10×), 25 µm (EZ). (C) Semi-quantitative VLDLR immunofluorescence (percentage of Ctrl; mean ± SEM; n = 3–5 litters/group). (D) Infrared scanner images for VLDLR (green), DRAQ5 (red), and merged coronal sections; Ctrl-, no primary antibody. (E) Quantification for VLDLR/DRAQ5 fluorescence ratios in the boxed ROI (% Ctl; mean ± SEM; n = 3–5 litters/group). (F) Immunoblot for VLDLR (~100 kDa) with β-actin (~42 kDa) control (top) and quantification (bottom) as % of Ctrl (mean ± SEM, n = 3 litters/group). Two-tailed unpaired Student's *t*-test; *p* values shown.

nisms. Although our transcriptomic and protein analyses indicate coherent attenuation of RELN and downstream effectors (ApoER2, VLDLR, and p-DAB1), the current evidence is correlative. Future studies using targeted manipulation of this pathway, such as in utero electroporation or viral-mediated RELN overexpression in diabetic embryos, will be informative to test whether restoring RELN signaling rescues neuronal migration and laminar organization. Complementary loss-of-function approaches (e.g., DAB1 or LRP8 knockdown in control embryos) could clarify whether the phenotypes observed here are specifically mediated by RELN pathway impairment versus broader metabolic consequences of maternal hyperglycemia. In addition, live imaging of neuronal migration in organotypic slice cultures from E12 to E16 cortices would allow direct visualization of radial and tangential migratory dynamics under diabetic conditions.

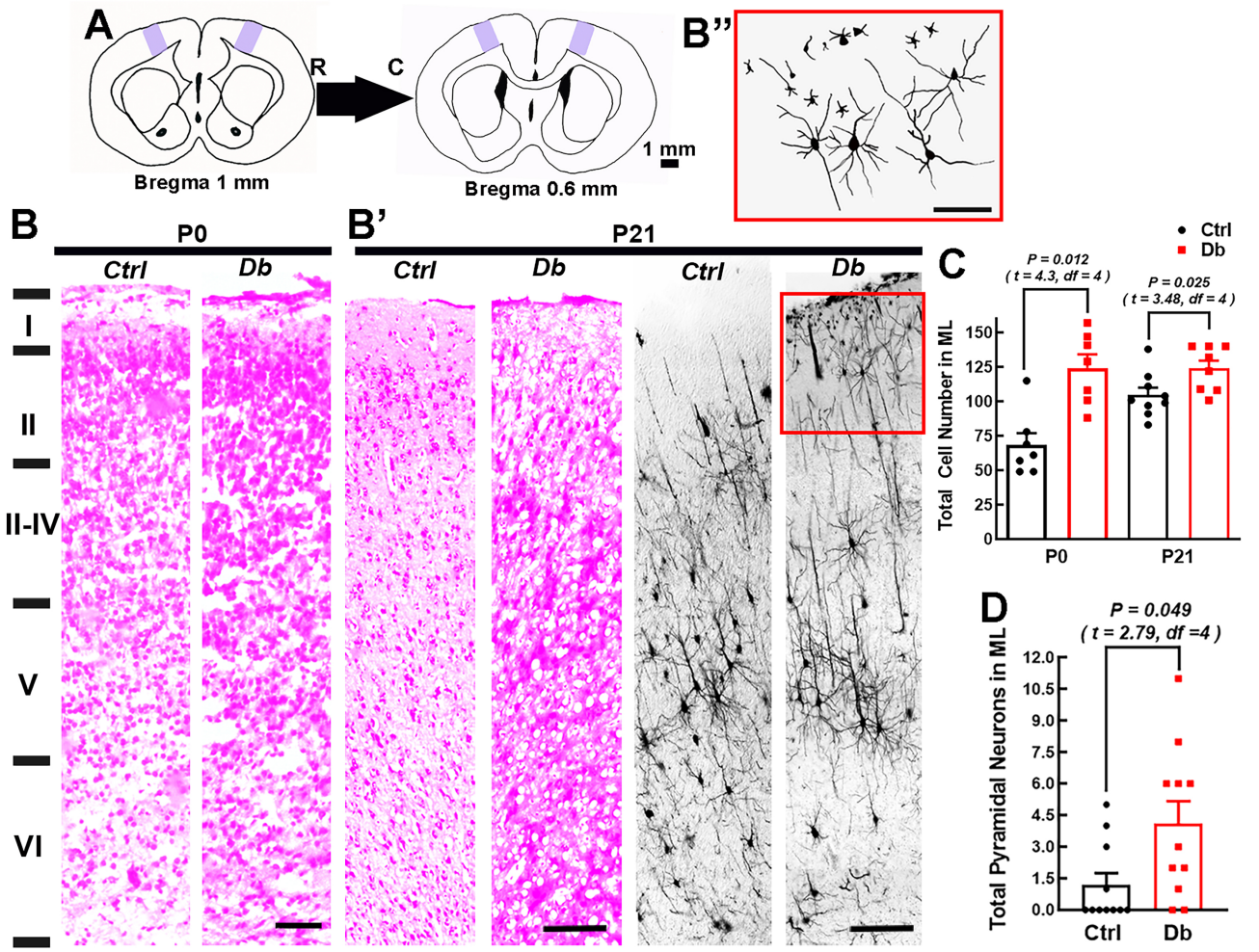

Fig. 7. Maternal hyperglycemia increases layer I cellularity and ectopic pyramidal neurons in M1. (A) Schematic of the rostro-caudal levels sampled (Bregma +1.0 to 0.6 mm; arrows indicate rostral (R) and caudal (C) directions. M1 is shaded purple. (B and B') Representative hematoxylin-eosin-stained coronal reconstructions of the M1 in P0 (B; two 10× fields) and P21 (B'; six 10× fields) offspring from control (Ctrl) and diabetic (Db) dams. (B' right) Representative Golgi-Cox reconstructions of P21 M1 (six 10× fields). The red box highlights ectopic layer I pyramidal neurons in Db. (B") Corresponding scaled drawing of ectopic neurons from Db (panel B'). Scale bars: A = 1 mm, B/B' = 250 µm; B" = 100 µm. The red box was used to identify ectopic pyramidal neurons in layer I. (C) Quantification of total cells in layer I at P0 and P21 (mean ± SEM; n = 3 litters/group with 2–3 offspring per litter; counts per matched ROI length/area-see Methods). Individual data points are shown. (D) Quantification of pyramidal neurons in layer I at P21 by Golgi-Cox (mean ± SEM; n = 3 each, with 3–4 offspring per litter). Individual data points are shown. Two-tailed unpaired Student's *t*-test; *p* values shown. Black dots (Ctrl) and red squares are data from the same animals. The biological replicate is the litter; when multiple pups per litter were analyzed, values were averaged to a single data point (n = 1) for that litter.

Importantly, our analysis was conducted exclusively in embryos without NTD, ensuring that the observed transcriptional and morphological alterations reflect consequences of hyperglycemia rather than a secondary effect of gross malformations. This distinction strengthens the interpretation of our data and underscores the value of this model for dissecting specific mechanisms of diabetic embryopathy. Integrating these mechanistic approaches will be essential to determine whether RELN hypofunction represents a primary pathogenic driver or a downstream outcome of altered progenitor proliferation and metabolic stress. Single-cell RNA-seq (scRNA-seq) in the cortical neuroepithelium from NTD-negative embryos will be particularly useful for resolving cell-type-specific changes in RELN-responsive neuroblasts and radial glial cells. As no such dataset is currently available. This approach will be necessary to test the precise hypothesis of whether RELN-expressing CRs and RELN-responsive neuroblasts/RGCs show selective transcriptional changes.

Regarding neurogenesis, our previous data suggest precocious/altered neurogenesis is associated with changes in the neural stem cell division patterns and in-

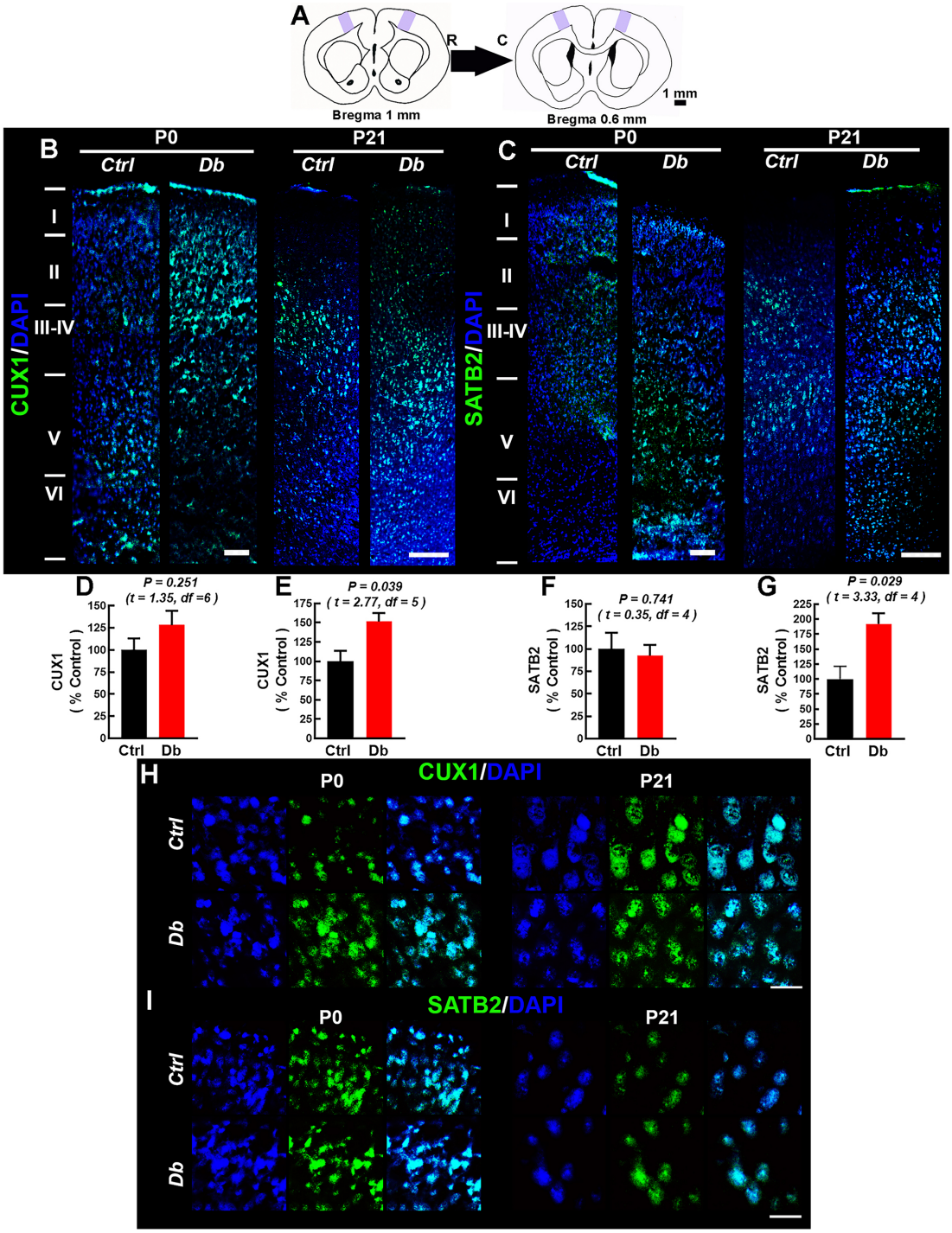

Fig. 8. Maternal hyperglycemia disrupts the distribution of CUX1 and SATB2 in M1 during early postnatal life. (A) Schematic showing the analyzed M1 region (purple) and Bregma +1.0 to +0.6 mm used for cytoarchitectonic sampling (R, rostral; C, caudal). (B,C) Representative 10× reconstructions of CUX1 (B) and SATB2 (C) immunofluorescence (green) with DAPI (blue) in P0 (three fields) and P21 (five fields) offspring from control (Ctrl) and diabetic (Db) dams (n = 3–5 litters at P0; n = 3 litters at P21). (D–G) Quantification of CUX1 (D,E) and SATB2 (F,G) immunofluorescence at P0 (D,F) and P21 (E,G) expressed as percentage of the Ctrl (mean ± SEM). Two-tailed unpaired Student's *t*-test; *p* values shown. (H,I) Representative micrographs (20×; 200% electronic Zoom) of DAPI-stained nuclei (blue), CUX1 and SATB2 (green) immunodetection from the upper layer, at postnatal day zero (P0, left) and P21 (right) from control (Ctrl) and diabetic (Db) groups. All the scale bars are 25 µm. CUX1, Cut Like Homeobox 1; SATB2, Special AT-Rich Sequence-Binding Protein 2.

creased expression of the high-molecular-weight isoform of microtubule-associated protein 2 (MAP2a/b). It is therefore plausible that both reduced RELN signaling and altered neurogenesis contribute to impaired migration and stratification. Systematic evaluation of layer-specific birthdating/markers across development (e.g., every 24 hours from E12 to E20) will help to determine whether inside-out layering is delayed or advanced.

The onset of maternal hyperglycemia at E5.5 may also influence earlier events, including initial neuroepithelial proliferation, which rapidly expands before E12. Disrupted dynamics at these stages could have durable effects on cortical size and architecture. Future studies examining E8–E10 (proliferation indices and mitotic regulators) together with DNA-damage and cell-death pathways will be important to determine whether maternal hyperglycemia perturbs neuroepithelium prior to the onset of robust corticogenesis, thereby predisposing to subsequent lamination defects. From a developmental-origin perspective, early RELN pathway inhibition provides a mechanistic bridge between diabetic pregnancy and long-term neurodevelopmental risk. Epidemiological data associate gestational diabetes with cognitive/motor impairment, language delays, attention-deficit/hyperactivity disorder, and autism spectrum disorder in offspring [19,21,23,25,34,35]; and human VLDLR variants have been linked to speech deficits and cerebellar hypoplasia [36,37]. While our structural and molecular data are compelling, future work should incorporate behavioral phenotyping (motor learning, skilled reach, cognitive assays) to connect circuit maldevelopment with function.

Recent transcriptomic and behavioral studies reinforce the long-term impact of maternal diabetes on offspring. For example, Aviel-Shekler and collaborators (2020) [35] reported that STZ-induced gestational diabetes at conception increases repetitive behaviors in adult male mice and alters gene expression in the frontal cortex and striatum. Frontal cortex differentially expressed genes were enriched for the function of forebrain development, and include genes implicated in the regulation of mammalian cortex size and organization, as well as the establishment of neuronal circuits (e.g., Nde1 and Bhlhe22) [35]. Interestingly, the authors state that glucose reached diabetic levels between E7 and E14, suggesting that maternal hyperglycemia, even when induced after implantation, can interfere with transcriptional programs governing neuronal differentiation and connectivity, consistent with our evidence of disrupted RELN signaling and abnormal radial migration in embryonic cortex. Future studies combining in utero manipulation of RELN signaling with longitudinal transcriptomic and postnatal behavioral assays will help establish the causal chain linking early cortical mispatterning to later cognitive and motor impairments.

Our study has several limitations. First, we used a streptozotocin-induced maternal hyperglycemia model that approximates, but does not replicate, the heterogeneity of human gestational diabetes; we did not measure maternal/fetal insulin or HbA1c, precluding dose-response inferences. Second, molecular readouts were primarily protein level and immunohistochemical; although transcriptomics guided pathway selection, we did not perform mechanistic rescue (e.g., recombinant RELN, receptor trafficking manipulation) nor direct test of the proposed miR-200-RELN axis. Third, the inference that reduced "stop" signaling causes layer I ectopias is correlative, as we did not quantify CRs number/activity, nor apoptosis of ectopic neurons, therefore, in future studies it will be crucial to perform p73 staining to confirm that the observed reduction in the RELN protein is due to reduced function/secretion rather than a loss or reduction of CRs. Fourth, some histological quantifications rely on 2D ROIs and immunofluorescence intensities, which can index both cell number and expression level; stereological estimates and per-layer cell densities would strengthen these conclusions. Fifth, we focused on E12/E16 and early postnatal M1 without behavioral endpoints; species/temporal differences may limit generalization to the human cortex. Finally, sex was not powered as a factor in all analyses. These constraints motivate future rescue and causal experiments.

Beyond radial migration, maternal hyperglycemia may also perturb tangential migration, which is required for the proper positioning of GABAergic interneurons from the medial and caudal ganglionic eminences. These neurons migrate through the intermediate and subventricular zones and integrate into the cortical plate circuit via guidance cues that include RELN, CXCL12/CXCR4, neuregulin/ErbB4, and semaphorins/plexin-Neuropilin pathways [38,39]. Disruption of these signals leads to abnormal interneuron distribution and an altered excitatory-inhibitory balance, potentially contributing to functional impairments in diabetic offspring. Because our analysis primarily addressed radial migration and laminar architecture, future work should map tangential routes to determine whether maternal hyperglycemia exerts broader effects on cortical circuit assembly.

In summary, maternal hyperglycemia is associated with attenuated RELN/DAB1 signaling, N-CAD mislocalization, impaired radial migration, and abnormal laminar architecture in postnatal life. These findings nominate the RELN pathway as a mechanistic node and a testable therapeutic target for mitigating neurodevelopmental sequelae in the offspring of diabetic pregnancies.

5. Conclusion

Our findings demonstrate that maternal hyperglycemia disrupts one of the most fundamental regulatory axes of corticogenesis: the RELN–DAB1 signaling pathway. By showing reduced levels of RELN, its receptors ApoER2 and VLDLR, and p-DAB1, together with N-CAD mislocalization, we provide evidence that from early to

late intrauterine development, the rat embryo may have compromised radial migration and cortical lamination. These alterations result in structural modifications during early postnatal life, characterized by ectopic pyramidal neurons and disorganized upper cortical layers in the M1.

From a developmental origins perspective, these results highlight how maternal diabetes can affect key molecular processes that guide neuronal positioning, potentially predisposing offspring to later cognitive and behavioral impairments. While our work was performed in a rat model, the parallels with human epidemiological data linking maternal diabetes to neurodevelopmental disorders strengthen the translational relevance.

Furthermore, our study identifies the RELN pathway as a mechanistic bridge between maternal hyperglycemia and abnormal cortical development. By pointing to this pathway as a potential experimental and therapeutic target, our findings encourage future investigations aimed at restoring RELN signaling or its downstream effectors to mitigate neurodevelopmental risks.

Availability of Data and Materials

All data generated or analyzed during this study are included in this published article and its supplementary materials. Original, western blot images and additional raw data supporting the conclusions of this study are available from the corresponding author upon request. Transcriptomic data is in https://www.ebi.ac.uk/fg/annotare/. (Accession number E-MTAB-15111)

Author Contributions

RVB and DAG wrote the original draft. DAG contributed to the conceptualization and discussion of the analyzed data. RVB and ISV performed the postnatal experiments, investigation, and analysis. RVB, DADP, VACP, and EVIH performed the prenatal experiments, investigation, and analysis. NFD and AMH contributed to the investigation, draft correction, and conceptualization. AMH contributed to the review and editing conception, design of the study, resources, and funding acquisition. All authors contributed to editorial changes in the manuscript. All authors read and approved the final manuscript. All authors have participated sufficiently in the work and agreed to be accountable for all aspects of the work.

Ethics Approval and Consent to Participate

This study was approved by the Institutional Committee for the Care and Use of Laboratory Animals (CICUAL) and the Research, Ethics, and Biosafety Committees of the Instituto Nacional de Perinatología (protocol number 2018-1-146). All experiments were carried out following the 'Guide for the Care and Use of Laboratory Animals' (NIH 80-23, revised 1978), the Official Mexican Standard for the Production, Care, and Use of Laboratory Animals (NOM-062-ZOO-1999), and the ARRIVE guidelines.

Acknowledgment

The authors thank Yuriria Paredes-Vivas and Heć-tor Herrera-Fernańdez for laboratory technical support and Talia Estrada-Rojas for animal care.

Funding

This research was funded by the Instituto Nacional de Perinatología (2018-1-146).

Conflict of Interest

The authors declare no conflict of interest.

Supplementary Material

Supplementary material associated with this article can be found, in the online version, at https://doi.org/10.31083/JIN46827.

References

[1] Molyneaux BJ, Arlotta P, Menezes JRL, Macklis JD. Neuronal subtype specification in the cerebral cortex. Nature Reviews. Neuroscience. 2007; 8: 427–437. https://doi.org/10.1038/nrn2151.

[2] Takiguchi-Hayashi K, Sekiguchi M, Ashigaki S, Takamatsu M, Hasegawa H, Suzuki-Migishima R, *et al*. Generation of reelin-positive marginal zone cells from the caudomedial wall of telencephalic vesicles. The Journal of Neuroscience: the Official Journal of the Society for Neuroscience. 2004; 24: 2286–2295. https://doi.org/10.1523/JNEUROSCI.4671-03.2004.

[3] López-Mengual A, Segura-Feliu M, Sunyer R, Sanz-Fraile H, Otero J, Mesquida-Veny F, *et al*. Involvement of Mechanical Cues in the Migration of Cajal-Retzius Cells in the Marginal Zone During Neocortical Development. Frontiers in Cell and Developmental Biology. 2022; 10: 886110. https://doi.org/10.3389/fcell.2022.886110.

[4] Cabrera-Socorro A, Hernandez-Acosta NC, Gonzalez-Gomez M, Meyer G. Comparative aspects of p73 and Reelin expression in Cajal-Retzius cells and the cortical hem in lizard, mouse and human. Brain Research. 2007; 1132: 59–70. https://doi.org/10.1016/j.brainres.2006.11.015.

[5] Hirota Y, Nakajima K. VLDLR is not essential for reelin-induced neuronal aggregation but suppresses neuronal invasion into the marginal zone. Development. 2020; 147: dev189936. https://doi.org/10.1242/dev.189936.

[6] Hack I, Hellwig S, Junghans D, Brunne B, Bock HH, Zhao S, *et al*. Divergent roles of ApoER2 and Vldlr in the migration of cortical neurons. Development (Cambridge, England). 2007; 134: 3883–3891. https://doi.org/10.1242/dev.005447.

[7] Jossin Y. Reelin Functions, Mechanisms of Action and Signaling Pathways During Brain Development and Maturation. Biomolecules. 2020; 10: 964. https://doi.org/10.3390/biom10060964.

[8] Hirota Y, Kubo KI, Katayama KI, Honda T, Fujino T, Yamamoto TT, *et al*. Reelin receptors ApoER2 and VLDLR are expressed in distinct spatiotemporal patterns in developing mouse cerebral cortex. The Journal of Comparative Neurology. 2015; 523: 463–478. https://doi.org/10.1002/cne.23691.

[9] Keshvara L, Benhayon D, Magdaleno S, Curran T. Identification of reelin-induced sites of tyrosyl phosphorylation on disabled 1. The Journal of Biological Chemistry. 2001; 276: 16008–16014. https://doi.org/10.1074/jbc.M101422200.

[10] Gao Z, Godbout R. Reelin-Disabled-1 signaling in neuronal mi-

gration: splicing takes the stage. Cellular and Molecular Life Sciences: CMLS. 2013; 70: 2319–2329. https://doi.org/10.1007/s00018-012-1171-6.

[11] Howell BW, Herrick TM, Hildebrand JD, Zhang Y, Cooper JA. Dab1 tyrosine phosphorylation sites relay positional signals during mouse brain development. Current Biology: CB. 2000; 10: 877–885. https://doi.org/10.1016/s0960-9822(00)00608-4.

[12] Ballif BA, Arnaud L, Arthur WT, Guris D, Imamoto A, Cooper JA. Activation of a Dab1/CrkL/C3G/Rap1 pathway in Reelin-stimulated neurons. Current Biology: CB. 2004; 14: 606–610. https://doi.org/10.1016/j.cub.2004.03.038.

[13] Hirota Y, Kubo KI, Fujino T, Yamamoto TT, Nakajima K. ApoER2 Controls Not Only Neuronal Migration in the Intermediate Zone But Also Termination of Migration in the Developing Cerebral Cortex. Cerebral Cortex (New York, N.Y.: 1991). 2018; 28: 223–235. https://doi.org/10.1093/cercor/bhw369.

[14] Brigman JL, Padukiewicz KE, Sutherland ML, Rothblat LA. Executive functions in the heterozygous reeler mouse model of schizophrenia. Behavioral Neuroscience. 2006; 120: 984–988. https://doi.org/10.1037/0735-7044.120.4.984.

[15] D'Arcangelo G, Miao GG, Chen SC, Soares HD, Morgan JI, Curran T. A protein related to extracellular matrix proteins deleted in the mouse mutant reeler. Nature. 1995; 374: 719–723. https://doi.org/10.1038/374719a0.

[16] Hadj-Sahraoui N, Frédéric F, Delhaye-Bouchaud N, Mariani J. Gender effect on Purkinje cell loss in the cerebellum of the heterozygous reeler mouse. Journal of Neurogenetics. 1996; 11: 45–58. https://doi.org/10.3109/01677069609107062.

[17] Valle-Bautista R, Márquez-Valadez B, Fragoso-Cabrera AD, García-López G, Díaz NF, Herrera-López G, *et al*. Impaired Cortical Cytoarchitecture and Reduced Excitability of Deep-Layer Neurons in the Offspring of Diabetic Rats. Frontiers in Cell and Developmental Biology. 2020; 8: 564561. https://doi.org/10.3389/fcell.2020.564561.

[18] Solís KH, Méndez LI, García-López G, Díaz NF, Portillo W, De Nova-Ocampo M, *et al*. The Histamine H1 Receptor Participates in the Increased Dorsal Telencephalic Neurogenesis in Embryos from Diabetic Rats. Frontiers in Neuroscience. 2017; 11: 676. https://doi.org/10.3389/fnins.2017.00676.

[19] Bolaños L, Matute E, Ramírez-Dueñas MDL, Zarabozo D. Neuropsychological Impairment in School-Aged Children Born to Mothers With Gestational Diabetes. Journal of Child Neurology. 2015; 30: 1616–1624. https://doi.org/10.1177/0883073815575574.

[20] Saito Y, Kobayashi S, Ito S, Miyashita C, Umazume T, Cho K, *et al*. Neurodevelopmental delay up to the age of 4 years in infants born to women with gestational diabetes mellitus: The Japan Environment and Children's Study. Journal of Diabetes Investigation. 2022; 13: 2054–2062. https://doi.org/10.1111/jdi.13907.

[21] Persson M, Tedroff K, Yin W, Andersson Franko M, Sandin S. Maternal type 1 diabetes, preterm birth, and risk of intellectual disability in the offspring: A nation-wide study in Sweden. European Psychiatry: the Journal of the Association of European Psychiatrists. 2024; 67: e11. https://doi.org/10.1192/j.eurpsy.2024.4.

[22] Buss C, Entringer S, Wadhwa PD. Fetal programming of brain development: intrauterine stress and susceptibility to psychopathology. Science Signaling. 2012; 5: pt7. https://doi.org/10.1126/scisignal.2003406.

[23] Camprubi Robles M, Campoy C, Garcia Fernandez L, Lopez-Pedrosa JM, Rueda R, Martin MJ. Maternal Diabetes and Cognitive Performance in the Offspring: A Systematic Review and Meta-Analysis. PloS One. 2015; 10: e0142583. https://doi.org/10.1371/journal.pone.0142583.

[24] Krakowiak P, Walker CK, Bremer AA, Baker AS, Ozonoff S, Hansen RL, *et al*. Maternal metabolic conditions and risk for autism and other neurodevelopmental disorders. Pediatrics. 2012; 129: e1121–e1128. https://doi.org/10.1542/peds.2011-2583.

[25] Chen KR, Yu T, Lien YJ, Chou YY, Kuo PL. Childhood neurodevelopmental disorders and maternal diabetes: A population-based cohort study. Developmental Medicine and Child Neurology. 2023; 65: 933–941. https://doi.org/10.1111/dmcn.15488.

[26] Bradford MM. A rapid and sensitive method for the quantitation of microgram quantities of protein utilizing the principle of protein-dye binding. Analytical Biochemistry. 1976; 72: 248–254. https://doi.org/10.1016/0003-2697(76)90527-3.

[27] Valle-Bautista R, de la Merced-García DS, Díaz-Piña DA, Díaz NF, Ávila-González D, Molina-Hernández A. Maternal diabetes disrupts early corticogenesis through altered mitotic gene regulation: a transcriptomic analysis. Frontiers in Endocrinology. 2025; 16: 1564441. https://doi.org/10.3389/fendo.2025.1564441.

[28] Clancy B, Darlington RB, Finlay BL. Translating developmental time across mammalian species. Neuroscience. 2001; 105: 7–17. https://doi.org/10.1016/s0306-4522(01)00171-3.

[29] Matsunaga Y, Noda M, Murakawa H, Hayashi K, Nagasaka A, Inoue S, *et al*. Reelin transiently promotes N-cadherin-dependent neuronal adhesion during mouse cortical development. Proceedings of the National Academy of Sciences of the United States of America. 2017; 114: 2048–2053. https://doi.org/10.1073/pnas.1615215114.

[30] Gil-Sanz C, Landeira B, Ramos C, Costa MR, Müller U. Proliferative defects and formation of a double cortex in mice lacking Mltt4 and Cdh2 in the dorsal telencephalon. The Journal of Neuroscience: the Official Journal of the Society for Neuroscience. 2014; 34: 10475–10487. https://doi.org/10.1523/JNEUROSCI.1793-14.2014.

[31] Stary CM, Xu L, Sun X, Ouyang YB, White RE, Leong J, *et al*. MicroRNA-200c contributes to injury from transient focal cerebral ischemia by targeting Reelin. Stroke. 2015; 46: 551–556. https://doi.org/10.1161/STROKEAHA.114.007041.

[32] Lamadrid-Romero M, Solís KH, Cruz-Reséndiz MS, Pérez JE, Díaz NF, Flores-Herrera H, *et al*. Central nervous system development-related microRNAs levels increase in the serum of gestational diabetic women during the first trimester of pregnancy. Neuroscience Research. 2018; 130: 8–22. https://doi.org/10.1016/j.neures.2017.08.003.

[33] Fu J, Tay SSW, Ling EA, Dheen ST. High glucose alters the expression of genes involved in proliferation and cell-fate specification of embryonic neural stem cells. Diabetologia. 2006; 49: 1027–1038. https://doi.org/10.1007/s00125-006-0153-3.

[34] Arabiat D, Jabery MA, Kemp V, Jenkins M, Whitehead LC, Adams G. Motor Developmental Outcomes in Children Exposed to Maternal Diabetes during Pregnancy: A Systematic Review and Meta-Analysis. International Journal of Environmental Research and Public Health. 2021; 18: 1699. https://doi.org/10.3390/ijerph18041699.

[35] Aviel-Shekler K, Hamshawi Y, Sirhan W, Getselter D, Srikanth KD, Malka A, *et al*. Gestational diabetes induces behavioral and brain gene transcription dysregulation in adult offspring. Translational Psychiatry. 2020; 10: 412. https://doi.org/10.1038/s41398-020-01096-7.

[36] Ferent J, Zaidi D, Francis F. Extracellular Control of Radial Glia Proliferation and Scaffolding During Cortical Development and Pathology. Frontiers in Cell and Developmental Biology. 2020; 8: 578341. https://doi.org/10.3389/fcell.2020.578341.

[37] Holling T, Abdelrazek IM, Elhady GM, Abd Elmaksoud M, Ryu SW, Abdalla E, *et al*. A homozygous nonsense variant in the alternatively spliced VLDLR exon 4 causes a neurodevelopmental disorder without features of VLDLR cerebellar hypoplasia. Journal of Human Genetics. 2024; 69: 623–628. https:

//doi.org/10.1038/s10038-024-01279-w.

[38] López-Bendito G, Sánchez-Alcañiz JA, Pla R, Borrell V, Picó E, Valdeolmillos M, *et al*. Chemokine signaling controls intracortical migration and final distribution of GABAergic interneurons. The Journal of Neuroscience: the Official Journal of the Society for Neuroscience. 2008; 28: 1613–1624. https://doi.org/10.1523/JNEUROSCI.4651-07.2008.

[39] Marín O, Yaron A, Bagri A, Tessier-Lavigne M, Rubenstein JL. Sorting of striatal and cortical interneurons regulated by semaphorin-neuropilin interactions. Science (New York, N.Y.). 2001; 293: 872–875. https://doi.org/10.1126/science.1061891.